Statistical Inference for Stochastic Processes **6:** 111–133, 2003.
© 2003 *Kluwer Academic Publishers. Printed in the Netherlands.*

Seasonal Space–Time Models for Climate Systems

XU-FENG NIU[1,*], IAN W. MCKEAGUE[1] and JAMES B. ELSNER[2]
[1]*Department of Statistics, Florida State University, Tallahassee, FL 32306, U.S.A.*
[2]*Department of Geography, Florida State University, Tallahassee, FL 32306, U.S.A.*

Abstract. A class of seasonal space–time models for general lattice systems is proposed. Covariance properties of spatial first-order models are studied. Estimation approaches in time series analysis are adopted and forecasting techniques using the seasonal space–time models are discussed. The models are applied to 516 consecutive fields of monthly averaged 500 mb geopotential heights over a 10×10 lattice in the extra-tropical northern hemisphere for the purpose of understanding the underlying statistical structure. It is found that space–time models with instantaneous spatial component give the best fit compared to other models in terms of maximizing the conditional likelihood function. The models are potentially useful for assessing the consistency of outputs from laboratory-based numerical models with field observations. Forecasting ability of the seasonal space–time models is also investigated.

AMS 1991 Subject Classification: Primary 62M10, 62M30; Secondary 60G15, 60G60.

Key words: covariance matrix function, longitudinal and latitudinal dependence, simultaneously specified space–time models, vector time series.

1. Introduction

Modeling and forecasting climate dynamical systems has a tremendous value to humanity. In the last two decades, record high temperatures and drought conditions in many regions around the world have prompted concern about the global greenhouse warming projected by sophisticated dynamical climate models (Hansen et al., 1988). Most recently, the frequency and severity of hurricanes and tornados in the United States and other parts of the world have also received heightened attention. In order to monitor future climate changes and compare climate data with laboratory-based model projections, an improved understanding of statistical structures of climate fields is urgently needed.

In this paper we propose a class of seasonal space–time models for describing and forecasting a climatologically important flow field consisting of monthly averaged geopotential heights. Geopotential heights of a constant pressure (isobaric) surface indicate the underlying air density with horizontal gradients of the heights approximating the horizontal momentum field through the geostrophic relationship

*Author for correspondence: Tel.: +1-850-644-4008; Fax: +1-850-644-5271; e-mail: niu@stat.fsu.edu

(Byers, 1974). Configurations of an isobaric surface determine the geostrophic vorticity, the advection of which is a crucial factor in middle latitude storm development. The statistical models developed here are useful for assessing the structural information of dynamical climate predictions. Although this study is motivated by modeling and forecasting the geopotential height field, the methodological techniques can be applied within other important disciplines such as geoscience, oceanography, ecology, and environmental science.

We shall fit the proposed space–time models to monthly averaged 500 mb geopotential height fields over a 10×10 lattice for the period January 1946 to December 1988. The 10×10 lattice covers the region latitudes 20°N–56°N and longitudes 66°W–120°W. Data are monthly averaged (based on twice-daily analyses) 500 hPa geopotential heights for a portion of the northern hemisphere compiled from the United States National Centers for Environmental Predictions (NCEP), and made available on CD from the University of Washington. The data were transformed from NCEP's octagonal grid to a 4° latitude $\times$ 6° longitude lattice using a cubic-spline interpolation for each time unit separately. The study region, shown in Figure 1, covers a large portion of the contiguous United States, Canada, and Mexico and represents a portion of the northern hemisphere for which reliable data are abundant.

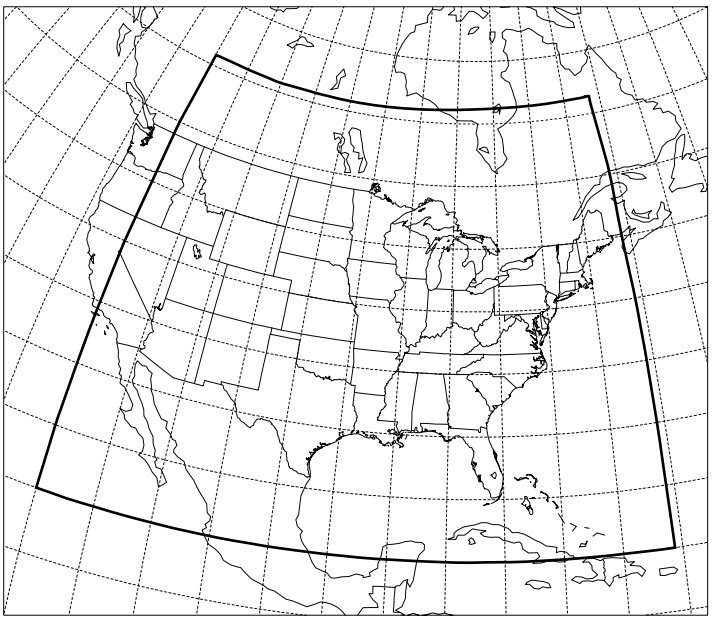

Figure 1. Region over which the space–time models are developed in this study. Lines of latitude and longitude are given every 5° with 25°N and 80°W located at the southeast tip of Florida. The 10×10 lattice is bounded by 20°N and 56°N latitude and by 66°W and 120°W longitude.

Space–time models suitable for describing the evolving random fields in climate and environmental systems have been developed by many researchers. For example, Cliff et al. (1975) proposed space–time autoregressive moving average (STARMA) models, which generalized both the ARMA time series models and the simultaneously specified spatial models introduced by Whittle (1954). Tjøstheim (1978, 1981, 1983) discussed unilateral causal (quadrant and half-space) models for high dimensional lattice systems. Basu and Reinsel (1993, 1994) investigated properties of spatial unilateral first-order ARMA models and regression models with spatially correlated errors. For space–time autoregressive (STAR) models, Ali (1979) developed a method to calculate the likelihood function for the parameters and briefly discussed the prediction problem. Most recently, Niu and Tiao (1995) developed a class of space–time regression models for the analysis of satellite data on a fixed latitude and applied the models to the total ozone mapping spectrometer (TOMS) data for trend assessment. Niu (1995) studied asymptotic properties of maximum likelihood estimates of parameters in these models, and proved consistency and asymptotic normality of the parameter estimates under mild conditions. Although the models of Niu and Tiao are parsimonious, with very few structural parameters, they do not allow latitudinal dependence – the proposed estimation procedure was specifically designed for a circular spatial process at a fixed latitude and does not apply to a general lattice system.

We now propose a class of seasonal space–time models on a rectangular lattice system that allow for latitudinal dependence and that are appropriate for modeling the geopotential height data, see Section 2. Various special cases of our models, designed to give parsimonious descriptions of the data, are examined in Section 3. For simplicity, we concentrate on submodels that have first-order spatial interactions in the sense that the value of the random field at a given site is influenced directly only by its nearest neighbors, and in a way that does not depend on the location of the site. Procedures for fitting the proposed models and obtaining predictions from them are presented in Section 4. The development of these procedures is based on a detailed study of the covariance structure of the model.

The atmosphere displays a great deal of variability in time and space, and it is hard to imagine that a single model for the whole climate system would be feasible. Our application of the proposed models to the geopotential height data is restricted to a relatively small region of the Earth's surface (Figure 1). We believe that the assumption of first-order spatial interactions holds up well over this region. The application is presented in Section 5.

2. Seasonal Space–Time Models for Lattice Systems

Climate observations on a fixed latitude–longitude grid can be considered as a lattice system. Climate lattice systems often show seasonal patterns in the temporal direction. For example, monthly time series usually have a seasonal period of 12 months. Consider a spatial and temporal process $\{Y_{ij}(t), i = 1, \ldots, m;$

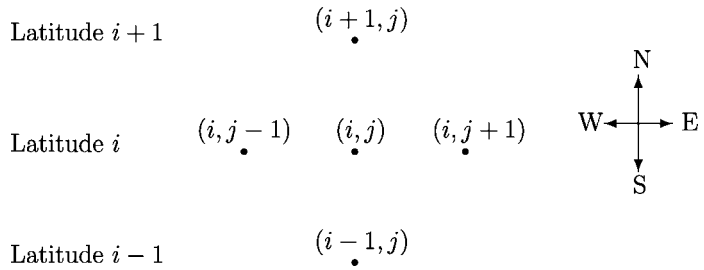

Figure 2. Labeling convention for lattice sites.

$j = 1, \ldots, n; t = 1, \ldots, T\}$ with sites (i, j) forming a two-dimensional regular grid $L_{m\times n}$ and with a seasonal period of s in the temporal direction. Label site (i, j) using i to index latitude and j to index longitude, see Figure 2; this is the reverse of the conventional site labeling used in spatial statistics, but more convenient in the present context. Specifically, for the 10×10 lattice shown in Figure 1, we define that latitudes 1–10 correspond to latitude zones 20°N, 24°N, ..., 56°N.

Let B be the temporal backward shift operator such that $BY_{ij}(t) = Y_{ij}(t-1)$. For a given site (i, j) in $L_{m\times n}$, define $N_{ij}(r) = \{(a, b) : (a, b) \in L_{m\times n}; 0 < \sqrt{(a-i)^2 + (b-j)^2} \leqslant r\}$ to be the order-r spatial neighborhood set centered at the site. Consider the following seasonal space–time model $\{Y_{ij}(t)\}$:

$$(1 - B^s)^D (1 - B)^d Y_{ij}(t) = \xi_{ij}(t), \tag{2.1}$$

and

$$\begin{aligned} \xi_{ij}(t) = {} & \sum_{k=0}^{p} \sum_{(a,b)\in N_{ij}(r)} \beta_{abk} \xi_{i-a,j-b}(t-k) + \\ & + \sum_{k=1}^{p} \phi_{ijk} \xi_{ij}(t-k) + \epsilon_{ij}(t) - \sum_{l=1}^{q} \theta_{ijl} \epsilon_{ij}(t-l). \end{aligned} \tag{2.2}$$

In model (2.1), the process $\{Y_{ij}(t)\}$ is first differenced temporally to remove possible seasonal patterns and trends; $d \geqslant 0$ is the number of trend differences, $s > 0$ is the seasonal period of $\{Y_{ij}(t)\}$, and $D \geqslant 0$ is the degree of seasonal differencing.

Model (2.2) gives the structure for the noise process $\{\xi_{ij}(t)\}$ in model (2.1) after trend and seasonal differencing. In the spatial direction, both longitudinal and latitudinal dependence are taking into account. In the temporal direction, (2.2) reduces to an autoregressive moving-average (ARMA) model with order p for the AR part and q for the MA part. The $\epsilon_{ij}(t)$'s are assumed to be independent $N(0, \sigma^2)$ random variables. The models in (2.1) and (2.2) will be called seasonal space–time autoregressive and moving-average models.

3. Covariance Properties of Space–Time Models

3.1. GENERAL COVARIANCE STRUCTURE

In this section, we obtain the reduced form representation of the space–time process $\{\boldsymbol{\xi}(t)\}$ specified in (2.2) and use it to find the covariance structure. Throughout the paper, we handle edge sites by equating unobserved border values to their respective means (see, e.g. Haining, 1978). Specifically, we set $\epsilon_{ij}(t) \equiv 0$ and $\xi_{ij}(t) \equiv 0$ if site (i, j) is outside the grid $L_{m\times n}$. In fact, it will be shown in this section that when the process $\{\xi_{ij}(t), t = 1, 2, \ldots, T\}$ is temporally stationary, the mean value of $\xi_{ij}(t)$ is zero.

For simplicity of presentation, only spatial first-order processes, that is, $r = 1$ in $N_{ij}(r)$, are considered. In this case, model (2.2) can be re-written in the form:

$$\begin{aligned}\xi_{ij}(t) \;=\; & \sum_{k=0}^{p}[\beta_{k1}\xi_{i-1,j}(t-k) + \beta_{k2}\xi_{i+1,j}(t-k) + \alpha_{k1}\xi_{i,j-1}(t-k) + \\ & + \alpha_{k2}\xi_{i,j+1}(t-k)] + \sum_{k=1}^{p}\phi_{ijk}\xi_{ij}(t-k) + \\ & + \epsilon_{ij}(t) - \sum_{l=1}^{q}\theta_{ijl}\epsilon_{ij}(t-l). \end{aligned} \tag{3.1}$$

Define

$$\boldsymbol{\xi}_j(t) = [\xi_{1j}(t), \xi_{2j}(t), \ldots, \xi_{mj}(t)]', \qquad \boldsymbol{\xi}(t) = [\boldsymbol{\xi}_1'(t), \boldsymbol{\xi}_2'(t), \ldots, \boldsymbol{\xi}_n'(t)]',$$
$$\boldsymbol{\epsilon}_j(t) = [\epsilon_{1j}(t), \epsilon_{2j}(t), \ldots, \epsilon_{mj}(t)]', \qquad \boldsymbol{\epsilon}(t) = [\boldsymbol{\epsilon}_1'(t), \boldsymbol{\epsilon}_2'(t), \ldots, \boldsymbol{\epsilon}_n'(t)]',$$

$$U_k = \begin{bmatrix} 0 & 1 & 0 & \ldots & 0 \\ 0 & 0 & 1 & \ldots & 0 \\ \cdots & \cdots & \cdots & \cdots & \cdots \\ 0 & 0 & 0 & \ldots & 1 \\ 0 & 0 & 0 & \ldots & 0 \end{bmatrix}_{k\times k} \qquad \text{for } k > 1,$$

$$\begin{aligned} \tilde{\Phi}_k &= \mathrm{Diag}(\phi_{11k}, \ldots, \phi_{m1k}, \phi_{12k}, \ldots, \phi_{m2k}, \ldots, \phi_{mnk}), \\ \tilde{\Theta}_l &= \mathrm{Diag}(\theta_{11l}, \ldots, \theta_{m1l}, \theta_{12l}, \ldots, \theta_{m2l}, \ldots, \theta_{mnl}), \\ A_0 &= I_{mn} - I_n \otimes [\beta_{01}U_m' + \beta_{02}U_m] - [\alpha_{01}U_n' + \alpha_{02}U_n] \otimes I_m, \\ A_k &= \tilde{\Phi}_k + I_n \otimes [\beta_{k1}U_m' + \beta_{k2}U_m] + [\alpha_{k1}U_n' + \alpha_{k2}U_n] \otimes I_m, \end{aligned}$$

where I_{mn} is the identity matrix with dimension mn and $A \otimes C = [a_{ij}C]$ denotes the Kronecker product of the matrices A and C. Using above notation, model (3.1) can be expressed as

$$A_0\boldsymbol{\xi}(t) = \sum_{k=1}^{p} A_k\boldsymbol{\xi}(t-k) + \boldsymbol{\epsilon}(t) - \sum_{l=1}^{q}\tilde{\Theta}_l\boldsymbol{\epsilon}(t-l). \tag{3.2}$$

Model (3.2) is a structural vector ARMA(p, q) model, which is called a simultaneous equation model in econometrics (see, e.g. Judge et al., 1985, Chapters 14–15). If the structure matrix A_0 is nonsingular, then model (3.2) can be written in a reduced form.

First, we study the invertibility of the structure matrix A_0. By Graybill (1983, pp. 284–285), $\beta_{01}U_m' + \beta_{02}U_m$ has distinct eigenvalues

$$\mu_{0i} = 2\sqrt{\beta_{01}\beta_{02}}\cos\left(\frac{i\pi}{m+1}\right), \quad i = 1, \ldots, m,$$

and $\alpha_{01}U_n' + \alpha_{02}U_n$ has distinct eigenvalues

$$\nu_{0j} = 2\sqrt{\alpha_{01}\alpha_{02}}\cos\left(\frac{j\pi}{n+1}\right), \quad j = 1, \ldots, n.$$

Define

$$\Lambda_{01} = \mathrm{Diag}(\mu_{01}, \ldots, \mu_{0m}), \qquad \Lambda_{02} = \mathrm{Diag}(\nu_{01}, \ldots, \nu_{0n}).$$

Then there are nonsingular matrices P_m and Q_n such that

$$\Lambda_{01} = P_m^{-1}(\beta_{01}U_m' + \beta_{02}U_m)P_m, \qquad \Lambda_{02} = Q_n^{-1}(\alpha_{01}U_n' + \alpha_{02}U_n)Q_n.$$

It is easy to see that

$$(Q_n^{-1} \otimes P_m^{-1})A_0(Q_n \otimes P_m) = I_{mn} - I_n \otimes \Lambda_{01} - \Lambda_{02} \otimes I_m,$$

where $\Lambda_0 = I_{mn} - I_n \otimes \Lambda_{01} - \Lambda_{02} \otimes I_m$ is a diagonal matrix. Therefore the eigenvalues of A_0 are

$$1 - \mu_{0i} - \nu_{0j} = 1 - 2\sqrt{\beta_{01}\beta_{02}}\cos\left(\frac{i\pi}{m+1}\right) - 2\sqrt{\alpha_{01}\alpha_{02}}\cos\left(\frac{j\pi}{n+1}\right),$$
$$i = 1, \ldots, m, \quad j = 1, \ldots, n.$$

When $(1 - \mu_{0i} - \nu_{0j}) \neq 0$ for $1 \leqslant i \leqslant m$ and $1 \leqslant j \leqslant n$, the matrix A_0 is invertible. In particular, A_0 is invertible if $\sqrt{\beta_{01}\beta_{02}} \leqslant 1/4$ and $\sqrt{\alpha_{01}\alpha_{02}} \leqslant 1/4$.

From now on, we assume that the structure matrix A_0 is invertible. Then model (3.1) can be written in the reduced form:

$$\boldsymbol{\xi}(t) = \sum_{k=1}^{p} A_0^{-1}A_k\boldsymbol{\xi}(t-k) + A_0^{-1}\boldsymbol{\epsilon}(t) - \sum_{l=1}^{q} A_0^{-1}\tilde{\Theta}_l\boldsymbol{\epsilon}(t-l). \tag{3.3}$$

Note that this representation implies the existence of the space–time process specified by (2.2).

Let

$$\Phi_k = A_0^{-1}A_k, \quad \text{for } 1 \leqslant k \leqslant p, \qquad \Phi(z) = I_{mn} - \sum_{k=1}^{p}\Phi_k z^k.$$

By the theory of vector time series (Hannan, 1970, Chapter 1), if $\det(\Phi(z)) \neq 0$ for all $|z| \leqslant 1$, then the process $\{\boldsymbol{\xi}(t)\}$ is temporally stationary and can be expressed in the causal form:

$$\boldsymbol{\xi}(t) = \sum_{k=0}^{\infty} \Psi_k \boldsymbol{\epsilon}(t-k), \tag{3.4}$$

which implies that $\boldsymbol{\xi}(t)$ is independent of $\{\boldsymbol{\epsilon}(t+1), \boldsymbol{\epsilon}(t+2), \ldots\}$ and $\mathrm{E}\boldsymbol{\xi}(t) = 0$. Define $\Theta_0 = A_0^{-1}$ and $\Theta_l = A_0^{-1}\tilde{\Theta}_l$ for $1 \leqslant l \leqslant q$. Then the matrices $\{\Psi_k\}$ can be calculated recursively from the equations:

$$\Psi_0 = \Theta_0, \qquad \Psi_k = \sum_{i=1}^{k} \Phi_i \Psi_{k-i} - \Theta_k \quad \text{for } k \geqslant 1, \tag{3.5}$$

where $\Phi_i = \mathbf{0}$ for $i > p$ and $\Theta_k = \mathbf{0}$ for $k > q$. By (3.4), the covariance matrix function $\Gamma(h) = \mathrm{Cov}(\boldsymbol{\xi}(t), \boldsymbol{\xi}(t+h)')$ has the form:

$$\Gamma(h) = \sigma^2 \sum_{k=0}^{\infty} \Psi_k \Psi'_{k+h} \quad \text{for } h = 0, \pm 1, \pm 2, \ldots. \tag{3.6}$$

In general, the process $\{\boldsymbol{\xi}(t)\}$ at a given time t is not spatially stationary since elements of the covariance matrix $\Gamma(0)$ may depend on spatial location.

3.2. COVARIANCE STRUCTURES OF SPECIAL CASES

We now discuss some special cases of model (3.1) for which the covariance matrices of $\{\boldsymbol{\xi}(t)\}$ can be expressed in more specialized forms. First, consider the following spatial first-order model:

$$\begin{aligned} \xi_{ij}(t) \;=\; & \sum_{k=0}^{p} [\beta_{k1}\xi_{i-1,j}(t-k) + \beta_{k2}\xi_{i+1,j}(t-k) + \\ & + \alpha_{k1}\xi_{i,j-1}(t-k) + \alpha_{k2}\xi_{i,j+1}(t-k)] + \\ & + \sum_{k=1}^{p} \phi_k \xi_{ij}(t-k) + \epsilon_{ij}(t) - \sum_{l=1}^{q} \theta_l \epsilon_{ij}(t-l). \end{aligned} \tag{3.7}$$

When $\beta_{k1} = \beta_{k2} \equiv \beta_k$ and $\alpha_{k1} = \alpha_{k2} \equiv \alpha_k$, model (3.7) is called a spatially symmetric model. In this case, we have

$$\begin{aligned} A_0 &= I_{mn} - I_n \otimes \beta_0[U'_m + U_m] - \alpha_0[U'_n + U_n] \otimes I_m, \\ A_k &= \phi_k I_{mn} + I_n \otimes \beta_k[U'_m + U_m] + \alpha_k[U'_n + U_n] \otimes I_m, \end{aligned}$$

and $\tilde{\Theta}_l = \theta_l I_{mn}$. It is easy to see that $\{A_k, k = 0, \ldots, p\}$ are symmetric matrices.

For first-order spatially symmetric models, the inverse of the matrix A_0 has an explicit form. First, notice that the eigenvalues of the matrix $U_n' + U_n$ are

$$\lambda_i = 2\cos\left(\frac{i\pi}{n+1}\right), \quad i = 1, \ldots, n.$$

When n is odd, $\lambda_{(n+1)/2} = 0$; when n is even, all the eigenvalues are not zero. For $\lambda_i \neq 0$, let δ_i and ω_i be the two roots of the equation $x^2 - \lambda_i x + 1 = 0$, that is,

$$\begin{aligned}\delta_i &= \cos\left(\frac{i\pi}{n+1}\right) + \sqrt{\cos^2\left(\frac{i\pi}{n+1}\right) - 1},\\ \omega_i &= \cos\left(\frac{i\pi}{n+1}\right) - \sqrt{\cos^2\left(\frac{i\pi}{n+1}\right) - 1}.\end{aligned}$$

Define $c_{ki} = (\delta_i^k - \omega_i^k)/(\delta_i - \omega_i)$ for $1 \leqslant k \leqslant n$. Then corresponding orthonormal eigenvectors of the λ_i's are given in the following theorem explicitly. The proof of this theorem is sketched in Appendix A.

THEOREM 3.1. *A normalized eigenvector corresponding to* $\lambda_i = 0$ *is*

$$\boldsymbol{p}_i = \left[\sqrt{\frac{2}{n+1}}, 0, -\sqrt{\frac{2}{n+1}}, 0, \sqrt{\frac{2}{n+1}}, 0, \ldots, 0, (-1)^{(n-1)/2}\sqrt{\frac{2}{n+1}}\right]',$$

where n is an odd integer. A normalized eigenvector corresponding to $\lambda_i \neq 0$ *is*

$$\boldsymbol{p}_i = \left[c_{1i}\sqrt{\sum_{k=1}^{n} c_{ki}^2},\ c_{2i}\sqrt{\sum_{k=1}^{n} c_{ki}^2}, \ldots,\ c_{ni}\sqrt{\sum_{k=1}^{n} c_{ki}^2}\right]'.$$

Let $P_n = [\boldsymbol{p}_1, \boldsymbol{p}_2, \ldots, \boldsymbol{p}_n]$. Then we have $P_n'(U_n' + U_n)P_n = \mathrm{Diag}(\lambda_1, \ldots, \lambda_n)$. Let P_m be an orthogonal matrix that diagonalize the matrix $(U_m' + U_m)$ and let $R = P_n \otimes P_m$. Then R is an orthogonal matrix and $R'A_0R = \Lambda_0$, where Λ_0 is a diagonal matrix with elements:

$$\begin{aligned}\lambda_0(i, j) &= 1 - \mu_{0i} - \nu_{0j} = 1 - 2\beta_0\cos\left(\frac{i\pi}{m+1}\right) - 2\alpha_0\cos\left(\frac{j\pi}{n+1}\right),\\ &\qquad i = 1, \ldots, m, \quad j = 1, \ldots, n.\end{aligned}$$

We assume that $\prod_{i=1}^m \prod_{j=1}^n (1 - \mu_{0i} - \nu_{0j}) \neq 0$, which implies that the matrix A_0 is invertible and the inverse is $A_0^{-1} = R\Lambda_0^{-1}R'$. Similarly, it is easy to see that $A_k = R\Lambda_k R'$, where Λ_k is a diagonal matrix with the elements:

$$\begin{aligned}\lambda_k(i, j) &= \phi_k - \mu_{ki} - \nu_{kj} = \phi_k - 2\beta_k\cos\left(\frac{i\pi}{m+1}\right) - 2\alpha_k\cos\left(\frac{j\pi}{n+1}\right),\\ &\qquad i = 1, \ldots, m, \quad j = 1, \ldots, n.\end{aligned}$$

For the case $p = 1$ and $q = 0$, we have

$$\boldsymbol{\xi}(t) = A_0^{-1} A_1 \boldsymbol{\xi}(t-1) + A_0^{-1} \boldsymbol{\epsilon}(t). \tag{3.8}$$

It is easy to see that $\Psi_k = [\Phi_1]^k A_0^{-1} = [A_0^{-1} A_1]^k A_0^{-1}$. Therefore

$$\Gamma(h) = \sigma^2 \sum_{k=0}^{\infty} \Psi_k \Psi_{k+h} = R[\Lambda(h)]R' \quad \text{for } h = 0, \pm 1, \pm 2, \ldots, \tag{3.9}$$

where $\Lambda(h)$ is a diagonal matrix with the elements:

$$\lambda(i, j) = \sum_{k=0}^{\infty} \lambda_0(i, j)^{-2k-h-2} \lambda_1(i, j)^{2k+h} = \frac{\lambda_1(i, j)^h \lambda_0(i, j)^{-2-h}}{1 - [\lambda_1(i, j)/\lambda_0(i, j)]^2}$$
$$\text{for } i = 1, \ldots, m, \quad j = 1, \ldots, n,$$

provided $|\lambda_1(i, j)/\lambda_0(i, j)| < 1$.

4. Prediction and Estimation

In this section, we assume that the process $\{\boldsymbol{\xi}(t)\}$ in (3.3) is temporally stationary and invertible. Forecasting techniques by using model (3.3) are discussed and estimation procedures for the parameters in the model are given. First, using the notation in Section 3.1, we can rewrite model (3.3) in the form:

$$\boldsymbol{\xi}(t) = \sum_{k=1}^{p} \Phi_k \boldsymbol{\xi}(t-k) + \Theta_0 \boldsymbol{\epsilon}(t) - \sum_{l=1}^{q} \Theta_l \boldsymbol{\epsilon}(t-l). \tag{4.1}$$

For any given time t, let $\hat{\boldsymbol{\xi}}_t(h)$ be the h-step ahead prediction defined by

$$\hat{\boldsymbol{\xi}}_t(h) = \mathrm{E}[\boldsymbol{\xi}(t+h) | \boldsymbol{\xi}(t), \boldsymbol{\xi}(t-1), \ldots, \boldsymbol{\xi}(1)] \quad \text{for } h \geqslant 1.$$

Then $\hat{\boldsymbol{\xi}}_t(h)$ is the best mean square predictor of $\boldsymbol{\xi}(t+h)$ given $\{\boldsymbol{\xi}(t), \ldots, \boldsymbol{\xi}(1)\}$. Since we assume normality of the process $\{\boldsymbol{\xi}(t)\}$, $\hat{\boldsymbol{\xi}}_t(h)$ coincides with the best linear predictor of $\boldsymbol{\xi}(t+h)$ given $\{\boldsymbol{\xi}(t), \ldots, \boldsymbol{\xi}(1)\}$.

Suppose that the process $\{\boldsymbol{\xi}(t)\}$ can be expressed in the causal form in (3.4). Let

$$\hat{\boldsymbol{\epsilon}}_t(j) = \mathrm{E}[\boldsymbol{\epsilon}(t+j) | \boldsymbol{\xi}(t), \boldsymbol{\xi}(t-1), \ldots, \boldsymbol{\xi}(1)] \quad \text{for } j \geqslant -q.$$

Then $\hat{\boldsymbol{\epsilon}}_t(j) = 0$ for $j \geqslant 1$. By model (4.1), the h-step ahead predictor $\hat{\boldsymbol{\xi}}_t(h)$ is

$$\hat{\boldsymbol{\xi}}_t(h) = \sum_{k=1}^{p} \hat{\Phi}_k \hat{\boldsymbol{\xi}}_t(h-k) - \sum_{l=1}^{q} \hat{\Theta}_l \hat{\boldsymbol{\epsilon}}_t(h-l) \quad \text{for } t > M \text{ and } h \geqslant 1, \tag{4.2}$$

where $\hat{\Phi}_k$ and $\hat{\Theta}_l$ are estimates of Φ_k and Θ_l, $M = \max(p, q)$, $\hat{\boldsymbol{\xi}}_t(h-k) = \boldsymbol{\xi}(t+h-k)$ for $(h-k) \leqslant 0$, and $\hat{\boldsymbol{\epsilon}}_t(j)$ can be estimated by $[\boldsymbol{\xi}(t+j) - \hat{\boldsymbol{\xi}}_{t+j-1}(1)]$ for $-q \leqslant j \leqslant 0$.

Let V_t be the one-step ahead prediction error covariance matrix, that is,

$$V_t = \mathrm{E}[\boldsymbol{\xi}(t+1) - \hat{\boldsymbol{\xi}}_t(1)][\boldsymbol{\xi}(t+1) - \hat{\boldsymbol{\xi}}_t(1)]'.$$

Algorithms for computing $\hat{\boldsymbol{\epsilon}}_t(\cdot)$, $\hat{\boldsymbol{\xi}}_t(h)$ and V_t have been developed in the time series literature (see, e.g. Brockwell and Davis, 1991, Chapter 11). In particular, for model (3.3) and large t, V_t can be estimated by $\sigma^2(A_0A_0')^{-1}$. If A_0 is nearly singular, then forecasts using space–time models with instantaneous spatial component will be unstable.

When observations $\boldsymbol{\xi} = [\boldsymbol{\xi}'(1), \ldots, \boldsymbol{\xi}'(T)]'$ are available, the parameters in the space–time model can be estimated using the maximum likelihood method. Specifically, let

$$\begin{aligned}
\boldsymbol{\beta} &= \{\beta_{abk}, (a,b) \in N_{ij}(h); 0 \leqslant k \leqslant p\},\\
\boldsymbol{\phi} &= \{\phi_{ijk}, 1 \leqslant i \leqslant m; 1 \leqslant j \leqslant n; 1 \leqslant k \leqslant p\},\\
\boldsymbol{\theta} &= \{\theta_{ijk}, 1 \leqslant i \leqslant m; 1 \leqslant j \leqslant n; 1 \leqslant k \leqslant p\}.
\end{aligned}$$

Then the exact log-likelihood function of the parameters is

$$l_{\mathrm{e}}(\boldsymbol{\beta}, \boldsymbol{\phi}, \boldsymbol{\theta}, \sigma^2) = -\frac{mnT}{2}\log(2\pi) - \frac{1}{2}\sum_{t=1}^{T}\log(|V_{t-1}|) - \frac{1}{2}S_T(\boldsymbol{\xi}), \tag{4.3}$$

where

$$S_{\mathrm{e}}(\boldsymbol{\xi}) = \sum_{t=1}^{T}[\boldsymbol{\xi}(t) - \hat{\boldsymbol{\xi}}_t(1)]'V_{t-1}^{-1}[\boldsymbol{\xi}(t) - \hat{\boldsymbol{\xi}}_t(1)].$$

Finding the maximum likelihood estimates of the parameters involves heavy computation. In practice, many approximations to the exact log-likelihood function are used to estimate the parameters. For example, using techniques similar to Niu and Tiao (1995), we can show that the conditional log-likelihood function given $\boldsymbol{\epsilon}(p|\boldsymbol{\xi}) = \cdots = \boldsymbol{\epsilon}(p+1-q|\boldsymbol{\xi}) = 0$ is

$$l_{\mathrm{c}}(\boldsymbol{\beta}, \boldsymbol{\phi}, \boldsymbol{\theta}, \sigma^2) \propto -(mnT - p)\log\sigma^2 + (T-p)\log|A_0|^2 - S_{\mathrm{c}}(\boldsymbol{\xi}), \tag{4.4}$$

where

$$\begin{aligned}
S_{\mathrm{c}}(\boldsymbol{\xi}) &= \frac{1}{\sigma^2}\sum_{t=p+1}^{T}[\boldsymbol{\epsilon}'(t|\boldsymbol{\xi})\boldsymbol{\epsilon}(t|\boldsymbol{\xi})],\\
\boldsymbol{\epsilon}(t|\boldsymbol{\xi}) &= A_0\boldsymbol{\xi}(t) - \sum_{k=1}^{p}A_k\boldsymbol{\xi}(t-k) + \sum_{l=1}^{q}\tilde{\Theta}_l\boldsymbol{\epsilon}(t-l|\boldsymbol{\xi}).
\end{aligned}$$

Compared with the exact log-likelihood function given in (4.3), the conditional log-likelihood function $l_{\mathrm{c}}(\boldsymbol{\beta}, \boldsymbol{\phi}, \boldsymbol{\theta}, \sigma^2)$ given in (4.4) is much easier to compute. For

large T, the difference between the two likelihood functions is negligible. From now on, the conditional likelihood estimates of the parameters will be denoted by $\hat{\boldsymbol{\beta}}, \hat{\boldsymbol{\phi}}, \hat{\boldsymbol{\theta}}$ and $\hat{\sigma}^2$, respectively.

5. Applications of the Seasonal Space–Time Models

At a given pressure level, the geopotential height fields over a time period form a space–time system, and spatial and temporal dependence of the data set should be examined for the purpose of understanding the statistical structure of this dynamical system. In this section, the seasonal space–time models are applied to 516 monthly averaged 500 mb geopotential height fields for the period January 1946 to December 1988 over the 10×10 lattice (Figure 1). Forecasting performance of different models will also be evaluated. Specifically, univariate time series and seasonal space–time models are built using the first 504 geopotential height fields, and the last 12 fields are used to compare the forecasting ability of different models.

Understanding statistical structures of midtropospheric geopotential height fields and improving the prediction accuracy of these fields are very important for medium-range (from 6 days to about 2 weeks) and long-range (monthly or seasonal outlooks) climate forecasting. Currently, medium- and long-range forecasts use time-averaged midtropospheric geopotential height fields as their primary guidance (see, e.g. Barnston and Livezey, 1987; Livezey and Schemm, 1988; Wagner, 1989). For instance, medium-range predictions for a certain period are usually based on a mean 500 mb height and anomaly field derived from a mix of output from two different numerical models with some statistical modifications added. Because of individual synoptic disturbances usually with a life cycle of about 3–7 days, the details of the weather are not predictable beyond 1–2 weeks (Epstein, 1988). The main concern of long-range forecasting is the general behavior of the larger scales of atmospheric circulation. As time ranges increased, Wagner (1989) pointed out that guidance for climate prediction increasingly relies on statistical techniques using autocorrelation fields rather than numerical weather prediction.

A number of meteorological operational and research organizations are now issuing seasonal to interannual climate outlooks based on significant improvements in coupled ocean–atmospheric general circulation modeling. The coupled general circulation model (GCM) is a dynamical system that mimics the dynamical system of the climate using equations for the ocean and the atmosphere. Modeling field observations of the climate system offers a method for validating the consistency of GCMs. For instance, comparisons can be made between variables (such as geopotential height) that are simulated from a GCM and field observations of the same variables (see Wigley et al., 1998). The autocovariance function of the observed variable should match the autocovariance of the GCM variable. If not, it implies faulty or incomplete dynamics in the GCM. As a potential application of the space–time models proposed in this study, we may fit the models to both field observations and numerical model outputs of a dynamical system and compare

the fitted models. Here we identify a way to go beyond using simply temporal statistics for comparisons to include space–time coupling and suggest models for better assessing the structural information of the next generation of GCMs.

5.1. UNIVARIATE TIME SERIES MODELS

Let $\{Y_{ij}(t), t = 1, \ldots, 516\}$ be the monthly averaged 500 mb geopotential heights observed at site (i, j). As a preliminary analysis, a univariate time series model is fitted to each of the 100 time series by using the well-known Box–Jenkins modeling procedure (Box and Jenkins, 1976). Figure 3(a) plots the geopotential heights in meters at site (1, 1) with latitude 20°N and longitude 120°W. The series shows a clear seasonal pattern with period 12 months, and the geopotential heights in years 1961 and 1962 were slightly higher than those in other years. Figure 3(b) shows the seasonally differenced series $\xi_{11}(t) = (1 - B^{12})Y_{11}(t) = Y_{11}(t) - Y_{11}(t - 12)$. Based on the Box–Jenkins modeling procedure, a univariate time series model with AR order $p = 1$ and an MA lag-12 term is identified for the seasonally differenced

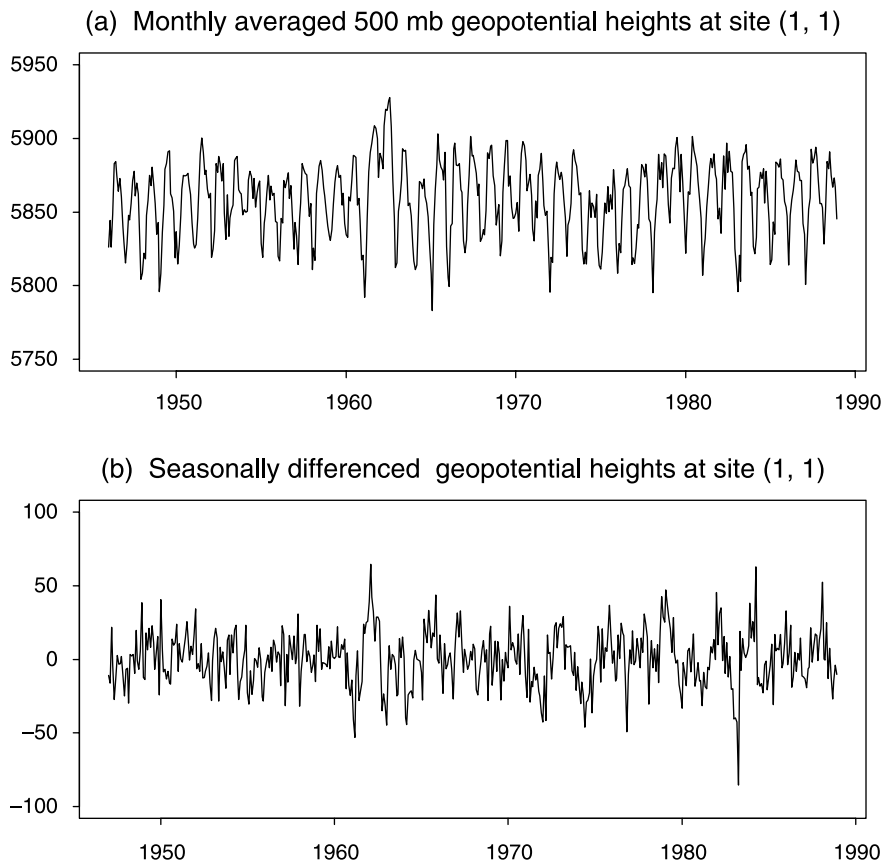

Figure 3. The geopotential height series at site (1, 1).

series, which is expressed in (5.1). When only temporal structure of the time series at site (1, 1) is concerned, diagnostic testings show that the fitted univariate model is adequate.

The same modeling procedure is performed to identify univariate time series models for geopotential heights at other sites. Almost all of the series follow the same model as that for the heights at site (1, 1), that is, the seasonally differenced series $\xi_{ij}(t) = Y_{ij}(t) - Y_{ij}(t-12)$ can be modeled in the form:

$$\xi_{ij}(t) = \phi_{ij}\xi_{ij}(t-1) + \epsilon_{ij}(t) - \theta_{ij}\epsilon_{ij}(t-12). \tag{5.1}$$

The estimated AR and MA coefficients in model (5.1) are plotted in Figure 4(a) and (b), respectively, where latitudes 1–10 correspond to 20°N–56°N with a 4° latitude interval. The 10 estimated AR coefficients for the height series on latitude 20°N have values around 0.5. When latitude increases from 20°N to 44°N, the estimated

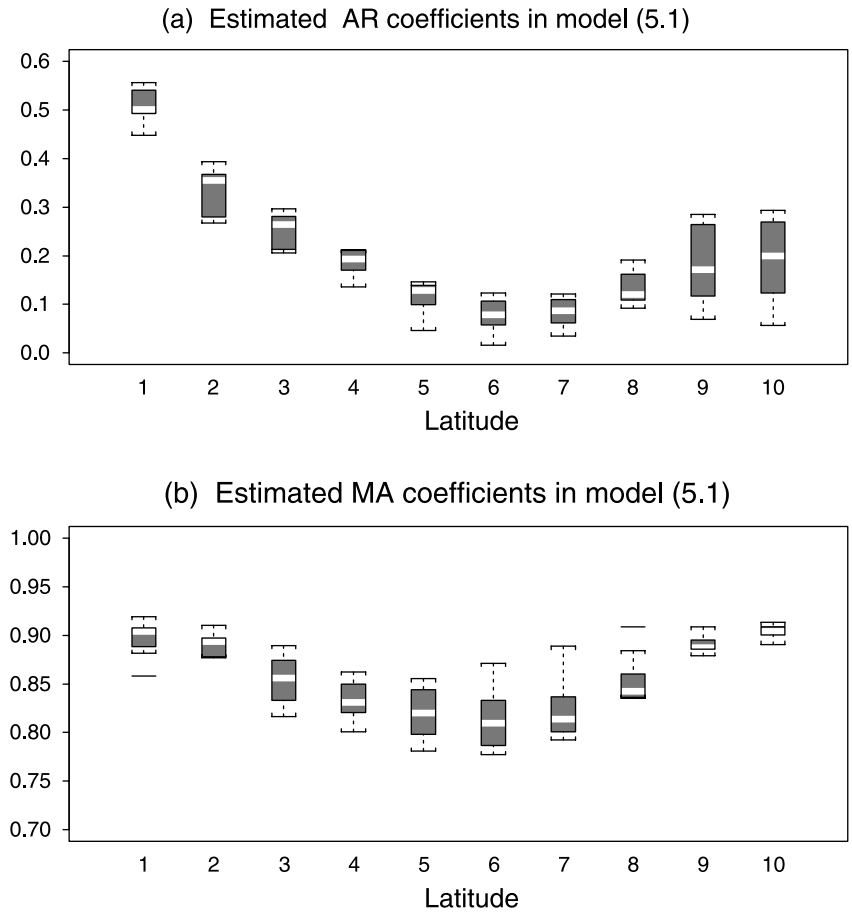

Figure 4. (a) and (b) Boxplots of the estimated AR and MA coefficients in model (5.1) plotted against latitude, where latitudes 1–10 corresponding to latitudes 20°N–56°N with a 4° interval.

AR coefficients show a decreasing pattern. In fact, in roughly half of the series at latitudes 36°N, 40°N and 44°N, the estimated AR coefficients are not significantly different from zero. The estimated MA coefficients range from 0.78 to 0.92, which have higher values for height series near the equator and the north pole and lower values for series on the mid-latitudes.

Notice from Figure 4(a) that the estimated AR coefficients $\{\hat{\phi}_{ij}, j = 1, 2, \ldots, 10\}$ on latitude i have about the same value. The estimated MA coefficients in Figure 4(b) show a similar pattern. Based on this observation, we may consider the following longitudinally homogeneous model for the geopotential height series:

$$\xi_{ij}(t) = \phi_i \xi_{ij}(t-1) + \epsilon_{ij}(t) - \theta_i \epsilon_{ij}(t-12). \tag{5.2}$$

Model (5.2) is actually a special case of the space–time model specified in (3.1). This model is fitted to the data set by using the first 504 geopotential height fields and parameters in the model are estimated by maximizing the conditional log-likelihood function given in (4.4). The estimated AR and MA coefficients along with their estimated standard errors are presented in Table I which shows that all the coefficients are significantly positive. For example, the estimated AR coefficient for latitude 45°N is 0.0816 with a t-value about 8.33, and this coefficient is roughly equal to the average of the estimated AR coefficients in model (5.1) for the 10 time series on the same latitude. The estimated MA coefficients for mid-latitudes are lower than those for latitudes near the equator and the north pole, which is similar to the pattern shown in Figure 4(b).

5.2. SPACE–TIME MODELS

Before building space–time models for the data set, we first examine spatial independence of the geopotential height fields. The univariate time series model in (5.1)

Table I. Parameter estimates in model (5.2)

Latitude	AR(1) coefficient $\hat{\phi}_i$	Standard error	MA coefficient $\hat{\theta}_i$	Standard error
20°N	0.4749	0.0286	0.8317	0.0329
24°N	0.3081	0.0230	0.8121	0.0254
28°N	0.2328	0.0172	0.7916	0.0182
32°N	0.1792	0.0132	0.7837	0.0138
36°N	0.1190	0.0110	0.7858	0.0110
40°N	0.0816	0.0098	0.7947	0.0098
44°N	0.1001	0.0091	0.8182	0.0093
48°N	0.1553	0.0083	0.8448	0.0085
52°N	0.1929	0.0075	0.8614	0.0076
56°N	0.1836	0.0067	0.8542	0.0069

is fitted to the geopotential height series at each site, and the sample covariance matrices $\{\hat{\Gamma}_\epsilon(h) = [\hat{\gamma}_{kl}(h)], h = 0, 1, \ldots, 10\}$ are calculated based on the residuals $\{\hat{\epsilon}_{ij}(t), i, j = 1, \ldots, 10; t = 1, \ldots, 504\}$. The sample cross-correlations $\hat{\rho}_{kl}(h)$'s corresponding to the process $\{\boldsymbol{\epsilon}(t)\}$ in model (5.1) are calculated by the formula (see, e.g. Brockwell and Davis, 1991, p. 406):

$$\hat{\rho}_{kl}(h) = \frac{\hat{\gamma}_{kl}(h)}{\sqrt{\hat{\gamma}_{kk}(0)\hat{\gamma}_{ll}(0)}} \quad \text{for } h = 0, \pm 1, \pm 2, \ldots.$$

In this study, sites (a, b) and (u, v) are said to be spatial neighbors of site (i, j) with the same order if the two sites have the same lattice separation from site (i, j). For a given h, the sample cross correlations $\hat{\rho}_{kl}(h)$'s can be grouped according to different spatial orders. Figure 5(a) shows the sample instantaneous spatial correlations of the process $\{\boldsymbol{\epsilon}_t\}$ in model (5.1) up to spatial order 10. It is clear from the plot that if the univariate time series model in (5.1) is fitted to the height series at each site separately, the instantaneous spatial correlations of the residuals are very strong. Figure 5(b) plots the lag-one spatial cross-correlations of the residuals, which shows only the order-one and order-two spatial correlations at temporal lag-one are slightly different from zero.

The strong instantaneous spatial dependence of the residuals from model (5.1) suggests that space–time models are needed for the geopotential height fields. First, we consider the following spatially symmetric first-order space–time model:

$$\begin{aligned} \xi_{ij}(t) &= \beta[\xi_{i-1,j}(t) + \xi_{i+1,j}(t)] + \alpha[\xi_{i,j-1}(t) + \xi_{i,j+1}(t)] + \\ &\quad + \phi_i \xi_{ij}(t-1) + \epsilon_{ij}(t) - \theta_i \epsilon_{ij}(t-12). \end{aligned} \tag{5.3}$$

Similar to model (5.2), the AR and MA coefficients in model (5.3) are assumed to depend only on latitude.

It is climatologically reasonable to assume a zonal (east–west) symmetry in the geopotential field under typical conditions of strong westerly flow (west–east) resulting from colder (more dense) air to the north and warmer (less dense) air to the south. North–south (meridional) symmetry occurs less often, but can occur with blocking patterns resulting in large temperature anomalies.

Model (5.3) is fitted to the data set and the parameters in the model are estimated by maximizing the conditional log-likelihood function in (4.4). The estimated spatial parameters are $\hat{\beta} = 0.271$ and $\hat{\alpha} = 0.317$, and both the estimated standard errors are about 0.001. The sample instantaneous spatial correlations and the sample lag-one cross correlations of the process $\{\boldsymbol{\epsilon}(t)\}$ in model (5.3) are calculated and presented in Figure 5(c) and (d). The sample instantaneous spatial correlations are apparently different from zero, which indicates that spatially nonsymmetric or higher-order space–time models are needed for this data set.

Next the following spatially nonsymmetric first-order space–time model is fitted to the series:

$$\begin{aligned} \xi_{ij}(t) &= \beta_{01}\xi_{i-1,j}(t) + \beta_{02}\xi_{i+1,j}(t) + \alpha_{01}\xi_{i,j-1}(t) + \alpha_{02}\xi_{i,j+1}(t) + \\ &\quad + \phi_i \xi_{ij}(t-1) + \epsilon_{ij}(t) - \theta_i \epsilon_{ij}(t-12). \end{aligned} \tag{5.4}$$

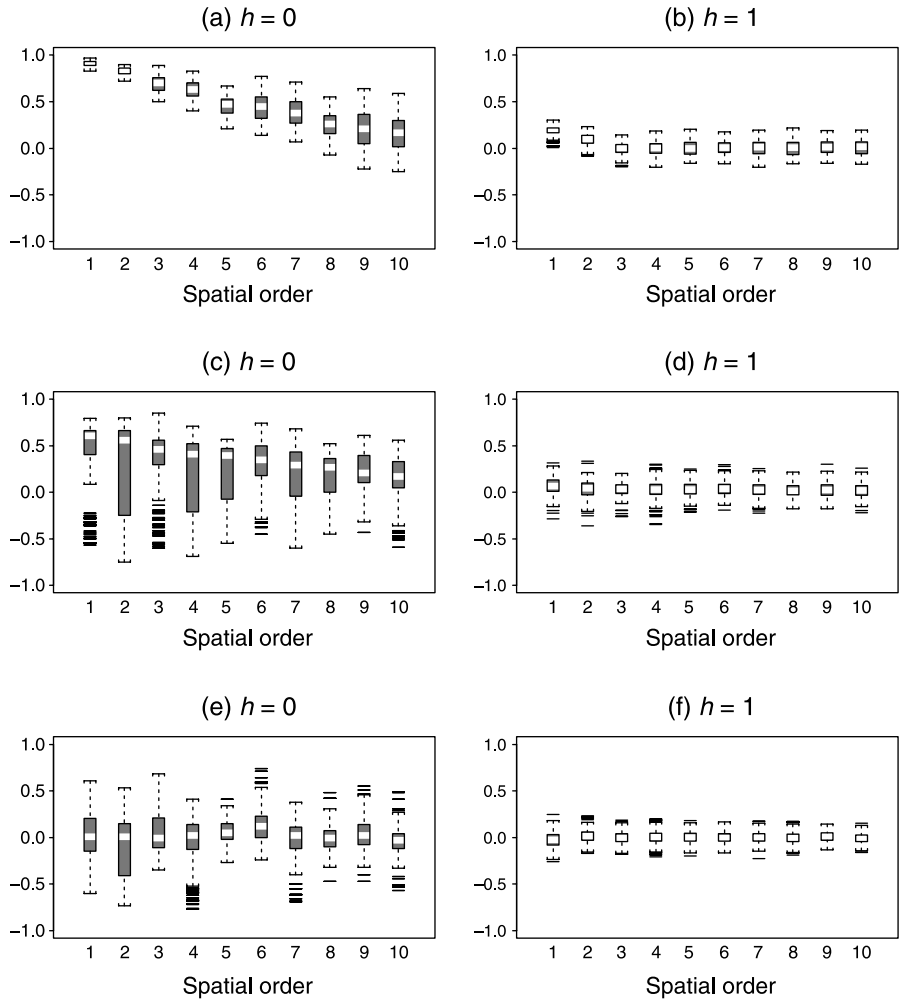

Figure 5. Sample spatial correlations at temporal lags $h = 0$ and $h = 1$ of the error process $\boldsymbol{\epsilon}(t)$ in different models, with (a) and (b) for model (5.1), (c) and (d) for model (5.3), and (e) and (f) for model (5.4).

The estimated spatial and temporal parameters in the above model are presented in Table II. The two latitudinal parameter estimates are $\hat{\beta}_{01} = 0.3798$, and $\hat{\beta}_{02} = 0.2237$, which indicates that a geopotential height series is more strongly correlated with a series at a site to the south than one to the north. Similarly, the two longitudinal parameter estimates indicate a stronger correlation with sites to the west than with sites to the east.

The estimated AR(1) coefficients for different latitudes shown in Table II are much smaller than those shown in Table I. For example, the estimated AR(1) coefficient for latitude 20°N based on model (5.4) is 0.1552 while the same coefficient based on model (5.2) is estimated to be 0.4749. This result indicates that the

Table II. Parameter estimates in the space–time model (5.4) (with the instantaneous spatial component)

Spatial coefficient estimates				
Coefficient	$\hat{\beta}_{01} = 0.3798$	$\hat{\beta}_{02} = 0.2237$	$\hat{\alpha}_{01} = 0.3250$	$\hat{\alpha}_{02} = 0.2570$
Standard error	0.0014	0.0010	0.0013	0.0012
Latitude	AR(1) coefficient $\hat{\phi}_i$	Standard error	MA coefficient $\hat{\theta}_i$	Standard error
Temporal coefficient estimates				
20°N	0.1552	0.0057	0.8371	0.0153
24°N	−0.0081	0.0044	0.7856	0.0229
28°N	−0.0070	0.0034	0.8460	0.0196
32°N	−0.0003	0.0026	0.8142	0.0165
36°N	−0.0010	0.0021	0.7925	0.0140
40°N	−0.0007	0.0018	0.8024	0.0125
44°N	0.0028	0.0017	0.8209	0.0113
48°N	0.0003	0.0016	0.8439	0.0100
52°N	−0.0042	0.0014	0.8522	0.0095
56°N	0.0372	0.0013	0.8256	0.0053

temporal correlations of the geopotential height observations become weaker after the instantaneous spatial dependence is taken into account. The estimated standard errors of the AR(1) coefficients based on model (5.4) are also much smaller than those based on model (5.2), which is mainly because the variance estimate $\hat{\sigma}^2$ of $\epsilon_{ij}(t)$ based on model (5.4) is much smaller than that based on model (5.2). On the other hand, the estimated MA coefficients at lag 12 from model (5.4) are about the same as those from model (5.2), which shows that including the instantaneous spatial component into the space–time models has very little impact on the temporal MA structure.

The sample spatial correlations of the process $\{\boldsymbol{\epsilon}(t)\}$ in model (5.4) are shown in Figure 5(e) and (f). The sample instantaneous spatial correlations for different spatial orders have medians around zero but with quite large ranges. Higher order space–time models have also been tried with no significant improvement in terms of reducing the instantaneous spatial correlations.

Two space–time models without instantaneous spatial component are also considered in this study. The first one is the following temporal lag-one and spatial first-order model:

$$\begin{aligned}\xi_{ij}(t) \;=\; & \beta_{11}\xi_{i-1,j}(t-1) + \beta_{12}\xi_{i+1,j}(t-1) + \\ & + \alpha_{11}\xi_{i,j-1}(t-1) + \alpha_{12}\xi_{i,j+1}(t-1) + \\ & + \phi_i\xi_{ij}(t-1) + \epsilon_{ij}(t) - \theta_i\epsilon_{ij}(t-12). \end{aligned} \tag{5.5}$$

In this model, the instantaneous component is replaced by the lag-one spatial component. The second model is the temporal lag-one and spatial second-order model which has the form:

$$\begin{aligned}\xi_{ij}(t) \;=\; & \beta_{11}\xi_{i-1,j}(t-1) + \beta_{12}\xi_{i+1,j}(t-1) + \\ & + \alpha_{11}\xi_{i,j-1}(t-1) + \alpha_{12}\xi_{i,j+1}(t-1) + \\ & + \beta_{13}\xi_{i-1,j-1}(t-1) + \beta_{14}\xi_{i+1,j-1}(t-1) + \alpha_{13}\xi_{i-1,j+1}(t-1) + \\ & + \alpha_{14}\xi_{i+1,j+1}(t-1) + \\ & + \phi_i\xi_{ij}(t-1) + \epsilon_{ij}(t) - \theta_i\epsilon_{ij}(t-12). \end{aligned} \tag{5.6}$$

Models (5.5) and (5.6) are fitted to the geopotential height fields. The estimated parameters in model (5.6), along with their estimated standard errors, are presented in Table III. The estimated first-order spatial coefficients are all negative, but the estimated temporal AR(1) coefficients and their standard errors based on model (5.6) are generally higher that those from model (5.2). For example, the estimated AR(1) coefficient for latitude 20°N based on model (5.6) is 0.6104 with an estimated standard error of 0.0395 while the same coefficient based on model (5.2) is estimated to be 0.4749 with an estimated standard error of 0.0286. The estimated temporal MA coefficients in models (5.6) and (5.2) are almost identical. A likelihood ratio test shows that model (5.6) is better than model (5.5). Several spatially higher order models were also tried, but showed no significant improvement over model (5.6) in terms of goodness-of-fit.

Values of the negative conditional log-likelihood function, $-l_c(\boldsymbol{\beta}, \boldsymbol{\alpha}, \boldsymbol{\phi}, \boldsymbol{\theta}, \sigma^2)$ are calculated at the estimated parameters for models (5.2)–(5.6). The values for models (5.3) and (5.4) are 3,518,077 and 3,088,586, respectively, which are much lower than the value of 84,609,229 for model (5.2). The likelihood ratio test shows that model (5.4) fits the data much better than models (5.3) and (5.2). On the other hand, the values for space–time models without instantaneous spatial component, (5.5) and (5.6), are 84,119,683 and 84,068,873, respectively, which are lower than the value 84,609,229 for model (5.2) but much higher than the values for models (5.3) and (5.4). It should be pointed out that models (5.3) and (5.4) are not nested in models (5.5) and (5.6). Based on these results, we conclude that the first-order space–time model in (5.4) with instantaneous spatial component provides the best fit for the 504 geopotential height fields in terms of maximizing the conditional likelihood function. Other space–time models with higher spatial orders have also been fitted to the data, but no significant improvements are shown by these models over model (5.4).

5.3. FORECASTING RESULTS

Based on the fitted models (5.1), (5.2), (5.5), and (5.6), the last 12 fields of the geopotential heights, $\{Y_{ij}(t), t = 505, \ldots, 516\}$ are forecasted. For a fixed h, the

Table III. Parameter estimates in the space–time model (5.6) (without the instantaneous spatial component)

Spatial coefficient estimates				
Order-one coefficient	$\hat{\beta}_{11} = -0.0527$	$\hat{\beta}_{12} = -0.0865$	$\hat{\alpha}_{11} = -0.0793$	$\hat{\alpha}_{12} = -0.0135$
Standard error	0.0264	0.0202	0.0261	0.0212
Order-two coefficient	$\hat{\beta}_{13} = 0.1654$	$\hat{\beta}_{14} = 0.0463$	$\hat{\alpha}_{13} = 0.0578$	$\hat{\alpha}_{14} = -0.0030$
Standard error	0.0204	0.0148	0.0169	0.0122
Latitude	AR(1) coefficient $\hat{\phi}_i$	Standard error	MA coefficient $\hat{\theta}_i$	Standard error
Temporal coefficient estimates				
20°N	0.6104	0.0395	0.8315	0.0272
24°N	0.3602	0.0397	0.8182	0.0202
28°N	0.2894	0.0373	0.7945	0.0151
32°N	0.2221	0.0362	0.7840	0.0115
36°N	0.1456	0.0355	0.7831	0.0094
40°N	0.0986	0.0353	0.7924	0.0081
44°N	0.1186	0.0353	0.8177	0.0076
48°N	0.1761	0.0352	0.8473	0.0068
52°N	0.2125	0.0351	0.8662	0.0062
56°N	0.1519	0.0335	0.8566	0.0056

sum of squared h-step ahead forecast errors is calculated by

$$\mathrm{SSFE}(h) = \sum_{i,j=1}^{10} [Y_{ij}(504+h) - \hat{Y}_{ij}(504+h)]^2 \quad \text{for } 1 \leqslant h \leqslant 12.$$

The total sum of squared forecast errors for each fitted model is calculated by $\mathrm{TSSFE} = \sum_{h=1}^{12} \mathrm{SSFE}(h)$. For the fitted model in (5.2), the TSSFE value is 1,450,355, which is slightly higher than the value 1,448,271 for the fitted model in (5.1). The TSSFE values for the fitted models in (5.5) and (5.6) are 1,420,981 and 1,417,860, respectively. Compared with models (5.1), (5.2), and (5.5), the temporal lag-one and spatial second-order in (5.6) gives the most accurate forecasts in terms of minimizing the TSSFE.

Proportions of the monthly variation in the last 12 geopotential height fields explained by different fitted models are calculated by the formula

$$PV = \frac{\sum_{h=1}^{12} \sum_{i,j=1}^{10} [\hat{Y}_{ij}(504+h) - \bar{Y})]^2}{\sum_{h=1}^{12} \sum_{i,j=1}^{10} [Y_{ij}(504+h) - \bar{Y})]^2},$$

where $\hat{Y}_{ij}(504+h)$ is the forecast value of $Y_{ij}(504+h)$ from a given fitted model and

$$\bar{Y} = \frac{\sum_{h=1}^{12} \sum_{i,j=1}^{10} Y_{ij}(504+h)}{1200}$$

is the average value of the last 12 geopotential height fields. The PV values explained by models (5.1) and (5.2) are about 90%. Forecasts from models (5.5) and (5.6) explain about 92 and 93% of the monthly variation in the observation, respectively.

It should be pointed out that the lag-one spatial dependence of the monthly averaged 500 mb height fields is not very strong, which is shown by the relatively small absolute values of the estimated spatial coefficients in model (5.6), see Table III. The weak lag-one spatial dependence explains why the predictive power of model (5.6) is only marginally better than that of the univariate time series model (5.1), although the improvement of forecast ability is still statistically significant. When daily or weekly observations are used instead of monthly data, it is expected that the lag-one spatial and temporal dependence of geopotential heights will be much stronger and substantial improvements in prediction can be achieved by using space–time models.

When the fitted space–time models (5.3) and (5.4) are used to forecast the last 12 geopotential height fields, the inverse structure matrix A_0^{-1} in (3.3) needs to be calculated. The minimum absolute eigenvalues of A_0 in models (5.3) and (5.4) are 0.0104 and 0.0233, respectively. These small minimum eigenvalues make the matrix A_0^{-1} unstable. In fact, forecasts of the last 12 geopotential height fields based on models (5.3) and (5.4), not presented in this paper, are worse than those from the other four fitted models because of inverse problems.

In Section 3.1, we pointed out that for the spatially nonsymmetric first-order space–time model (3.1), a sufficient condition for the structure matrix A_0 to be invertible is $\sqrt{\beta_{01}\beta_{02}} \leqslant 1/4$ and $\sqrt{\alpha_{01}\alpha_{02}} \leqslant 1/4$. For model (5.4), we have $\sqrt{\hat{\beta}_{01}\hat{\beta}_{02}} = \sqrt{0.3798 \times 0.2237} \approx 0.29$ and $\sqrt{\hat{\alpha}_{01}\hat{\alpha}_{02}} = \sqrt{0.3250 \times 0.2570} \approx 0.289$, that is, the sufficient condition does not hold empirically. In this case, the estimated structure matrix A_0 is nearly singular even though still invertible. Based on our experience, unlike lagged spatial and temporal correlations, strong instantaneous spatial dependence of a process is not particularly helpful for improving forecasting ability in the temporal direction.

In this study, we find that the spatial–temporal dependence of the seasonally differenced monthly averaged 500 mb geopotential height fields, over the 10×10 lattice for the period January 1946 to December 1988, can be described by the space–time model given in (5.4). This result is valuable for extracting structural information on climate lattice systems. If one is interested in specific features concerning spatial and temporal data sets, such as long-term trends and seasonal patterns, this type of model should be used. For instance, the space–time models are potentially useful for comparing the structural information of variables from field observations and from outputs of GCMs.

We also find that some space–time models with instantaneous spatial component, such as models (5.3) and (5.4) in this study, may perform poorly in forecasting due to inverse problems. Compared with other models, seasonal space–time model (5.6) without instantaneous spatial component provides more accurate forecasts for the monthly averaged 500 mb geopotential height fields. Techniques developed in this study can be applied to model and forecast geopotential heights at different pressure levels. Then the predicted height fields can serve as guidance for improving long-range climate forecasting.

Appendix A. Proof of Theorem 3.1

Proof of Theorem 3.1. A normalized eigenvector $\boldsymbol{p}_i = [p_{i1}, \ldots, p_{in}]'$ corresponding to the eigenvalue λ_i satisfies the following conditions:

$$(U_n' + U_n)\boldsymbol{p}_i = \lambda_i \boldsymbol{p}_i, \qquad \sum_{k=1}^{n} p_{ik}^2 = 1. \tag{A.1}$$

Let $p_{i0} = 0$, then Equation (A.1) can be written as

$$p_{ik} - \lambda_i p_{i,k-1} + p_{i,k-2} = 0 \quad \text{for } 2 \leqslant k \leqslant n, \qquad \sum_{k=1}^{n} p_{ik}^2 = 1. \tag{A.2}$$

For n odd and $\lambda_i = 0$, it is easy to see that $p_{i2} = p_{i4} = \cdots = p_{i,n-1} = 0$ and $p_{ik} = (-1)^{(k-1)/2} p_{i1}$ for k odd. Therefore we have $[(n+1)/2]p_{i1}^2 = 1$. Choose

$p_{i1} = \sqrt{2/(n+1)}$. Then

$$\boldsymbol{p}_i = \left[\sqrt{\frac{2}{n+1}}, 0, -\sqrt{\frac{2}{n+1}}, 0, \sqrt{\frac{2}{n+1}}, 0, \ldots, 0, (-1)^{(n-1)/2}\sqrt{\frac{2}{n+1}}\right]'$$

is a normalized eigenvector for $\lambda_i = 0$.

For $\lambda_i \neq 0$, notice that $\delta_i + \omega_i = \lambda_i$ and $\delta_i\omega_i = 1$. The equation $p_{ik} - \lambda_i p_{i,k-1} + p_{i,k-2} = 0$ can be written in the form

$$p_{ik} - \delta_i p_{i,k-1} = \omega_i(p_{i,k-1} - \delta_i p_{i,k-2}),$$

which implies that $p_{ik} - \delta_i p_{i,k-1} = \omega_i^{k-2}(p_{i2} - \delta_i p_{i1})$. Since $p_{i2} = \lambda_i p_{i1}$, we have

$$p_{ik} - \delta_i p_{i,k-1} = \omega_i^{k-2}(\lambda_i - \delta_i)p_{i1} = \omega_i^{k-1}p_{i1}. \tag{A.3}$$

Similarly we have

$$p_{ik} - \omega_i p_{i,k-1} = \delta_i^{k-2}(\lambda_i - \omega_i)p_{i1} = \delta_i^{k-1}p_{i1}. \tag{A.4}$$

$[\delta_i \times (\text{A.4}) - \omega_i \times (\text{A.3})]$ gives us

$$p_{ik} = \frac{\delta_i^k - \omega_i^k}{\delta_i - \omega_i}p_{i1} = c_{ik}p_{i1}. \tag{A.5}$$

Notice that

$$\begin{aligned}(\delta_i^k - \omega_i^k) - \lambda_i(\delta_i^{k-1} - \omega_i^{k-1}) &= (\delta_i^k - \omega_i^k) - (\delta_i + \omega_i)(\delta_i^{k-1} - \omega_i^{k-1}) \\ &= \delta_i\omega_i^{k-1} - \omega_i\delta_i^{k-1} = -(\delta_i^{k-2} - \omega_i^{k-2}),\end{aligned}$$

which follows that the coefficients c_{ik} satisfy the recursive equation $c_{ik} = \lambda_i c_{i,k-1} - c_{i,k-2}$ for $k \geqslant 3$. Since $c_{i1} = 1$ and $c_{i2} = \lambda_i$, the coefficients c_{ik} are all real numbers.

Finally, the p_{ik}'s satisfy the normalization equation

$$\sum_{k=1}^{n} p_{ik}^2 = p_{i1}^2 \sum_{k=1}^{n} c_{ik}^2 = 1.$$

Choosing $p_{i1} = \sqrt{1/\sum_{k=1}^{n} c_{ik}^2}$, then we have

$$\boldsymbol{p}_i = \left[c_{1i}\sqrt{\sum_{k=1}^{n} c_{ki}^2}, c_{2i}\sqrt{\sum_{k=1}^{n} c_{ki}^2}, \ldots, c_{ni}\sqrt{\sum_{k=1}^{n} c_{ki}^2}\right]'.$$

□

Acknowledgments

This research was partially supported by NSF Grant ATM-9417528. The authors would like to thank the editor, and the three referees for their valuable comments and suggestions.

References

Ali, M. M.: Analysis of stationary spatial–temporal processes: estimation and prediction, *Biometrika* **66** (1979), 513–518.

Barnston, A. G. and Livezey, R. E.: Classification, seasonality and persistence of low-frequency atmospheric circulation patterns, *Monthly Weather Rev.* **115** (1987), 1083–1126.

Basu, S. and Reinsel, G. C.: Properties of the spatial unilateral first-order ARMA model, *Adv. Appl. Probab.* **25** (1993), 631–648.

Basu, S. and Reinsel, G. C.: Regression models with spatially correlated errors, *J. Am. Statist. Assoc.* **89** (1994), 88–99.

Box, G. E. P. and Jenkins, G. M.: *Time Series Analysis: Forecasting and Control*, Holden-Day, Inc., 1976.

Brockwell, P. J. and Davis, R. A.: *Time Series Theory and Methods*, 2nd edition, Springer, New York, 1991.

Byers, H. R.: *General Meteorology*, 4th edition, McGraw-Hill, New York, 1974.

Cliff, A. D., Haggett, P., Ord, J. K., Bassett, K. A. and Davies, R. B.: *Elements of Spatial Structure: A Quantitative Approach*, Cambridge University Press, New York, 1975.

Epstein, E. S.: Long-range weather prediction: limits of predictability and beyond, *Weather and Forecasting* **3** (1988), 69–75.

Graybill, F. A.: *Matrices with Applications in Statistics*, 2nd edition, Wadsworth, Inc., 1983.

Haining, R. P.: The moving average model for spatial interaction, *Trans. Inst. Br. Geogr. N.S.* **3** (1978), 202–225.

Hannan, E. J.: *Multiple Time Series*, Wiley, New York, 1970.

Hansen, J., Fung, J., Lacis, A., Rind, D., Lebedeff, S., Ruedy, R., Russell, G. and Stone, P.: Global climate changes as forecast by Goddard Institute for space studies three-dimensional model, *J. Geophys. Res.* **93** (1988), 9341–9364.

Judge, G. G., Griffiths, W. E., Hill, R. C., Lütkepohl, H. and Lee, T.-C.: *The Theory and Practice of Econometrics*, Wiley, New York, 1985.

Livezey, R. E. and Schemm J.-K.: The relative utility of persistence and medium-range dynamic forecasts of monthly mean 700 mb heights, *Monthly Weather Rev.* **116** (1988), 266–268.

Niu, X.-F.: Asymptotic properties of maximum likelihood estimates in a class of space–time models, *J. Multivariate Anal.* **55** (1995), 82–104.

Niu, X.-F. and Tiao, G. C.: Modeling satellite ozone data, *J. Am. Statist. Assoc.* **90** (1995), 969–983.

Tjøstheim, D.: Statistical spatial series modeling, *Adv. Appl. Probab.* **10** (1978), 130–154.

Tjøstheim, D.: Autoregressive modeling and spectral analysis of array data in the plane, *IEEE Trans. Geosci. Remote Sensing* **GE19** (1981), 15–24.

Tjøstheim, D.: Statistical spatial series modeling II. Some further results on unilateral processes, *Adv. Appl. Probab.* **15** (1983), 562–584.

Wagner, A. J.: Medium- and long-range forecasting, *Weather and Forecasting* **4** (1989), 413–426.

Whittle, P.: On stationary processes in the plane, *Biometrika* **41** (1954), 434–449.

Wigley, T. M. L., Smith, L. R. and Santer, B. D.: Anthropogenic influence on the autocorrelation structure of hemispheric-mean temperatures, *Science* **282** (1998), 1676–1679.